Research Article Vol. 4, No. 9 / September 2017 / Optica 1080

Biomaterial microlasers implantable in the cornea, skin, and blood

Matjaž Humar,[1,2,3,*] Anja Dobravec,[1] Xiangwei Zhao,[4] and Seok Hyun Yun[3,5]

[1]Condensed Matter Department, J. Stefan Institute, Jamova 39, SI-1000 Ljubljana, Slovenia
[2]Faculty of Mathematics and Physics, University of Ljubljana, Jadranska 19, SI-1000 Ljubljana, Slovenia
[3]Wellman Center for Photomedicine, Harvard Medical School, Massachusetts General Hospital, 65 Landsdowne St. UP-5, Cambridge, Massachusetts 02139, USA
[4]State Key Laboratory of Bioelectronics, School of Biological Science & Medical Engineering, Southeast University, Nanjing 210096, China
[5]Harvard-MIT Health Sciences and Technology, Cambridge, 77 Massachusetts Avenue Cambridge, Massachusetts 02139, USA
*Corresponding author: matjaz.humar@ijs.si

Received 1 June 2017; revised 27 July 2017; accepted 1 August 2017 (Doc. ID 297238); published 7 September 2017

Fluorescent stand-alone laser particles that are implantable into biological tissues have the potential to enable novel optical imaging, diagnosis, and therapy. Here we demonstrate several types of biocompatible microlasers and their lasing action within biological systems. Dye-doped polystyrene beads were embedded in the cornea and optically pumped to generate narrowband emission. We fabricated microbeads with poly(lactic-co-glycolic acid) and poly(lactic acid)-substances approved for medical use-and demonstrate lasing from within tissues and whole blood. Furthermore, we demonstrate biocompatible cholesterol-derivative microdroplet lasers via self-assembly to an onion-like radially resonant photonic crystal structure. These types of implanted lasers may enable real-time monitoring of physiological information, such as temperature. © 2017 Optical Society of America

OCIS codes: (140.2050) Dye lasers; (140.3945) Microcavities; (160.1435) Biomaterials; (160.3710) Liquid crystals.

https://doi.org/10.1364/OPTICA.4.001080

1. INTRODUCTION

Recently there has been an increasing interest in bio-lasers [1,2]. Lasers have several advantages over fluorescence, including narrow emission linewidth, high coherence, large intensity, and highly nonlinear output. These properties have been harnessed for ultrasensitive sensing [3], spectral multiplexing [4], and sub-diffraction microscopy [5]. Examples of biological lasers include hybrid lasers containing cells [6,7] and tissues [8] inside Fabry–Perot cavities, microlasers inside cells [4,9], random lasers [10] in tissues [11], and spasers in cells and tissues [12]. Lasers made entirely from biomaterials were also demonstrated. For example, a distributed feedback laser (DFB) was made from riboflavin-doped gelatin [13] and silk [14], and whispering-gallery-mode (WGM) lasing has been achieved in water droplets [15,16] and protein microspheres [17].

We have investigated the feasibility of implanting stand-alone bio-lasers into tissues. With exception of random lasers [11] and spasers [12], studies on implantable, stand-alone lasers have been lacking [18]. The spasers are of nano size, which facilitates their use for biological applications. Their operation has been demonstrated both inside cells and *in vivo* by injections into a mouse ear. Because of very narrow linewidth and multimode lasing, WGM lasers may be more suitable for sensing [19] and barcoding [20] in comparison to random lasers and spasers. Here we demonstrate the laser action of polymeric microlasers embedded in the cornea, skin, and whole blood. In addition to chasing a long-standing curiosity about super humans, such as living lasers capable of emitting lasers from their eyes, the underlying motivation of this study is for potential applications to sensing and diagnosis. For example, implanted lasers in the biological tissues may provide physiological information [21], such as glucose and temperature, in real time.

An important step toward implantable lasers is to achieve biocompatibility; that is, the lasers should not cause immune reactions and foreign-body responses beyond acceptable levels. In some cases, it may be desirable that the lasers are made from biological materials and are biodegradable. For example, WGM lasers were made of bovine serum albumin (BSA) protein and polysaccharides derived from plants [22]. Most of the current bio-integrated lasers, however, contain some non-biodegradable or medically untested materials. In this paper, we employed transparent polymers poly(lactic-co-glycolic acid) (PLGA) and poly (lactic acid) (PLA). Both materials are already approved for medical use and routinely used in clinics for medical implants, sutures, and drug delivery, and recently have also been used to make implantable optical waveguides [23]. Microparticles for drug delivery are made from these polymers [24,25], which already have spherical shape and size suitable for sustaining WGMs. We have also explored photonic crystal lasers made from biocompatible, self-assembling liquid crystal chiral molecules. Unlike synthetic liquid crystals extensively used for photonic applications

[26,27], cholesterol derivatives [28], specifically cholesteryl esters, are biocompatible [29,30] and found in the human body. Here we demonstrate that droplets of cholesterol derivatives emit laser light and can be used as temperature sensors.

2. RESULTS

A. Polystyrene Bead Lasers in the Cornea

To demonstrate WGM lasing in tissue, we first used bovine cornea, which is transparent. The refractive index of the cornea is ~1.37–1.38. Commercially available green fluorescent polystyrene beads (Thermo Scientific, Fluoro-Max, 8 μm mean diameter, 18% coefficient of variation) were used, which are inert but not biodegradable. A dispersion of these beads in phosphate buffered saline (PBS) with a concentration 2×10^6 beads/ml was used for injection. Bovine eye globes were acquired from a local distributor and the experiments were performed within less than 10 h postmortem. A hypodermic needle (30 gauge, 0.3 mm outer diameter) was used for the injection of the bead dispersion into the bovine cornea. The needle was inserted at a shallow angle not to penetrate beyond the cornea [Fig. 1(a)]. The needle was slowly retracted from the cornea while at the same time the bead dispersion was pushed out of the needle with a slight pressure. The beads were deposited along the path of the needle [Fig. 1(b)]. For the pumping of the lasers and the collection of light, a 20 × 0.45 NA objective was used [Fig. 1(c)]. The microlasers were pumped by an optical parametric oscillator with 5 ns pulse duration, tuned to 475 nm and repetition rate 10 Hz. The laser beam was slightly divergent at the objective entrance pupil, so that the focus at the sample was located slightly further away from the objective focal plane, producing a 20 μm wide excitation area in the focal plane. The collected light was sent through a dichroic mirror to a camera or an imaging spectrometer (300 mm focal length, 0.05 nm resolution). This same optical setup was also used for all the following results. When a single bead was optically pumped, the output showed lasing characteristics, namely, a sharp intensity threshold and narrowband (<0.2 nm) laser lines [Fig. 1(d)]. In general, the lasing was very similar as has been shown for the same beads inside cells [4], including lasing spectra at different pump intensities and the laser threshold (~4 nJ).

B. Biodegradable Polymer Microbeads and Lasing in the Blood

To make biodegradable lasers, we have produced PLA and PLGA spheres by the standard oil in water dispersion procedure. PLA (Hycail CML-PLA, MW of $63,000 \pm 12,000$ Da) or PLGA (Sigma, ester-terminated lactide:glycolide 75:25 with a MW of 76,000–115,000 Da) was dissolved in dichloromethane (DCM) at a concentration of 4 wt. %. Nile Red was added to the DCM solution at a concentration of 1 mM. The water phase was prepared by dissolving 1 wt. % polyvinyl alcohol (Mowiol 4-88, Mw of ~31,000 Da) in water as a surfactant to stabilize the droplet dispersion. The DCM solution was added at 1% to the water phase and vigorously shaken to produce polydispersed droplets. Droplets were ultrasonicated in an ultrasonic bath at the lowest power setting for 10 min. The dispersion was left for at least 15 h so the DCM evaporated from the mixture, leaving solid spheres. The final concentration of Nile Red in solid PLA or PLGA beads was 25 mM. The beads were washed several times with water to remove the PVA, with centrifugation at 2500 g between the washing steps. Beads created by this procedure had sizes ranging from 10 μm to several 100 μm [Figs. 2(a) and 2(b)]. In particular, larger PLA spheres had some porosity in the center, but smooth nonporous surfaces. Upon pumping with a green pulsed laser (frequency doubled Nd:YAG laser at 532 nm with 1 ns pulse duration, repetition 10 Hz), clear peaks appeared in the emission spectrum from single beads [Figs. 2(c) and 2(d)], corresponding to WGM lasing. The emission intensity versus input energy

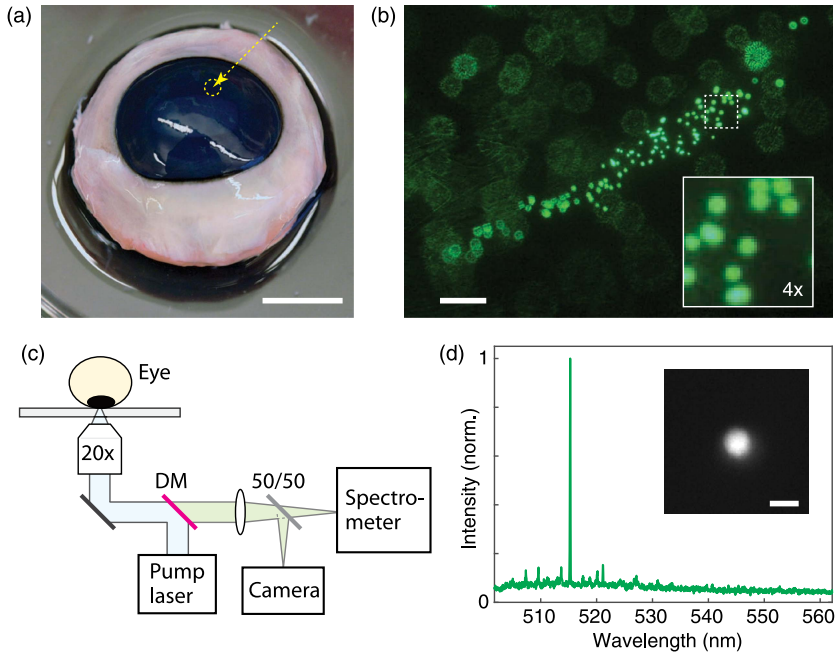

Fig. 1. Lasing of polystyrene beads in bovine cornea. (a) Site of injection of the bead dispersion. (b) Fluorescence image of the injected beads. The out-of-focus beads are on the eye surface. (c) Optical setup. (d) Lasing spectrum of a single illuminated bead (inset) inside the bovine cornea. Scale bars, 20 mm in (a), 200 μm in (b), and 10 μm in (d).

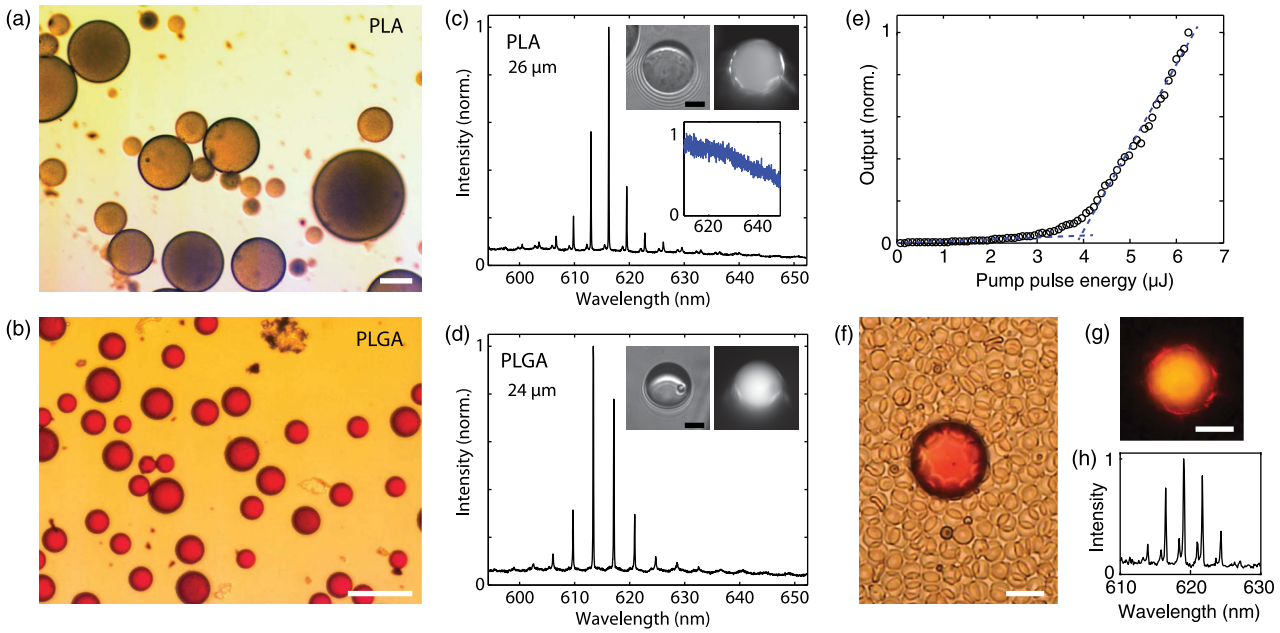

Fig. 2. Whispering gallery mode lasers made from biodegradable polymers. (a) PLA beads doped with Nile Red. (b) PLGA beads doped with Nile Red. (c) Lasing spectrum of a single 26 μm PLA bead in water. Bright-field image (left inset) and lasing (right inset). Spectrum from a 15 μm bead, which is not lasing (bottom inset). The spontaneous emission spectrum is the same as the fluorescence spectrum from the dye used. (d) Lasing spectrum of a single 26 μm PLGA bead in water. Bright-field image (left inset) and lasing (right inset). (e) Output of PLA as the pump energy is increased shows typical threshold behavior. (f) A 40 μm diameter PLA bead in blood. The bead is surrounded by red blood cells. (g) Lasing of the same PLA bead in blood and (h) the emission spectrum. Scale bars are 100 μm in (a) and (b), 10 μm in (c) and (d), and 20 μm in (f) and (g).

clearly shows a threshold behavior [Fig. 2(e)]. The minimum size for lasing was approximately 20 μm, limited by the radiation leakage, which is highly dependent on refractive index difference between the laser and the exterior as well as the size. PLA and PLGA polymers have a refractive index of 1.47, lower than polystyrene (1.59).

The operation of these lasers in human blood was tested. Dispersion of PLA beads in PBS was mixed in ratio of 1:1 with freshly collected whole human blood [Fig. 2(f)]. The mixture was introduced in between two glass slides and imaged within 15 min after blood collection. PLA lasers, surrounded by approximately 4 times smaller red blood cells, showed lasing [Fig. 2(g)] with narrow lines in the emission spectrum [Fig. 2(h)]. With blood only, no measurable fluorescence emission was detected. PLGA lasers showed lasing inside blood, as well. Lasing in blood was as efficient as in water, meaning that the red blood cells and other constituents of blood did not frustrate lasing. Bio-lasers in blood could enable diagnosis to be performed directly in blood [31].

C. Polymer Microlasers in the Skin

To study the lasing properties of polymer mirolasers in biological tissues [Fig. 3(a)], we have implanted the above-described PLA beads dispersed in phosphate buffered saline into porcine skin tissues using a tattoo machine [Fig. 3(b)]. Pig skin was purchased from a local supplier and kept in PBS until use. A dense bead suspension containing almost no water was deposited on the skin surface. A tattoo machine with needles at the end was passed a few times across the skin where the beads were deposited. The tattoo machine is composed of a bundle of several (3–9) non-hollow needles mounted on a bar. An electromagnet vibrates the bar up and down along its axis with a typical amplitude of 2 mm. The needles penetrate the skin and, at the same time, push the ink below the skin. The tattoo machine was operated at frequency of ~100 Hz while moving along the surface of the skin to

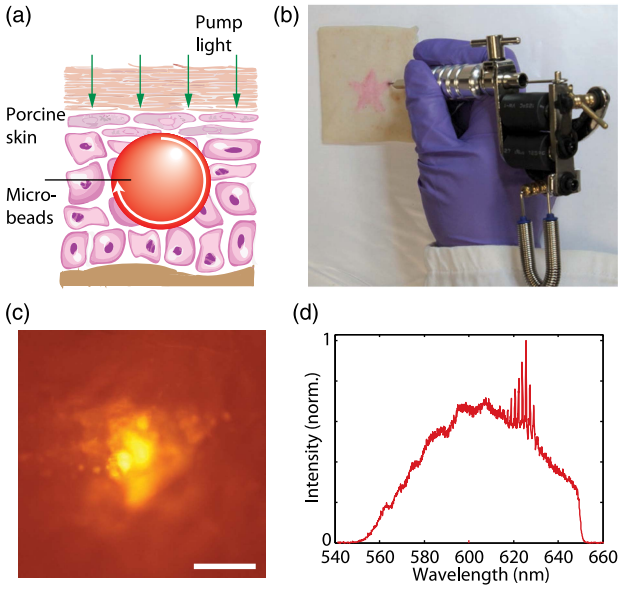

Fig. 3. Lasers implanted into skin. (a) Principle of operation of a laser in skin tissue. (b) Implantation of lasers into porcine skin using a standard tattoo machine. (c) Light from a laser embedded approximately 100 μm below the skin surface. Because of light scattering, the laser itself cannot be clearly distinguished. (d) Output spectrum from Fig. 3(c) showing WGM laser peaks at 615–625 nm superimposed on a broad fluorescent background. Scale bar, 50 μm in (c).

create the desired spatial patterns and, at the same time, the skin was repeatedly stretched so that larger beads could also penetrate the holes formed by the needles. The beads remaining on the surface were removed by washing with PBS. Alternatively, hypodermic needles with appropriate inner diameters could be used for injection of the beads. We examined a single bead implanted at a depth of approximately 100 μm below the skin surface. When it was illuminated by the external laser (frequency doubled Nd:YAG laser at 532 nm with 1 ns pulse duration, repetition 10 Hz) a clear fluorescence emission was observed, but the spherical shape of the laser could not be discerned due to light scattering of the skin [Fig. 3(c)]. In the emission spectrum from the center of the illumination, clear lasing peaks can be distinguished above the broad background fluorescence [Fig. 3(d)]. The background is largely autofluorescence of the skin tissue. The broad peaks from 550 to 620 nm are caused by the non-uniform transmission spectrum of the dichroic mirror. From the WGM output spectrum, the bead size was determined to be 49.8 μm.

D. Cholesterol Bragg Onion Microlasers

We used cholesterol derivatives to form an onion-like, spherical photonic crystal structure in a droplet [Fig. 4(a)]. The periodic structure selectively reflects light in accordance with Bragg's law. The cholesteric mixture was prepared from cholesteryl nonanoate, cholesteryl oleyl carbonate, and cholesteryl chloride in ratio of 5:4:3. The ratio was optimized so that the long bandedge matched the maximum emission of the fluorescent dye. The reflection was measured by introducing a thin layer of the mixture in between two glass slides, and the spectrum of white light reflected from the layer was measured with a spectrometer [Fig. 4(b)]. Pyrromethene 580 (BODIPY) fluorescent dye was introduced into the mixture at a concentration of 2 wt. %. All four components were heated up to 90°C so that the cholesterol derivatives reached the isotropic phase (phase transition at 63°C), and the mixture was mixed for 15 min. The mixture was cooled to room temperature and centrifuged at 10,000 g for 5 min to remove any undissolved dye or other particulates. A small quantity of the cholesterol mixture (~1 μl) was introduced into 0.5 ml of glycerol and stirred with a pipette tip to form droplets. Under crossed polarizers, the droplets have a cross structure, indicating a good liquid crystal orientation throughout the whole droplet volume [Fig. 4(c)]. The molecules are oriented tangentially in each shell and form a helical twist from the center out toward the surface in all directions. Closer inspection reveals a line extending from the center of the droplet to the surface [Fig. 4(d)]. This is a defect structure that is formed for topological reasons [32,33]. Namely, a sphere cannot be combed without introducing at least one defect, where the orientation of the molecules is undefined.

When a cholesterol droplet was illuminated with an external pulsed laser (frequency-doubled Nd:YAG laser at 532 nm with 1 ns pulse duration, repetition 10 Hz), laser emission was visible from the center of the droplet [Fig. 4(e)]. In the emitted spectrum, one or two lines are visible, corresponding to bandedge lasing on the short and long edges of the photonic bandgap [Fig. 4(f)]. Which line will be lasing depends on the positions of the two edges relative to the gain of the dye. One of the advantages of photonic crystal lasers is that the lasing wavelength is

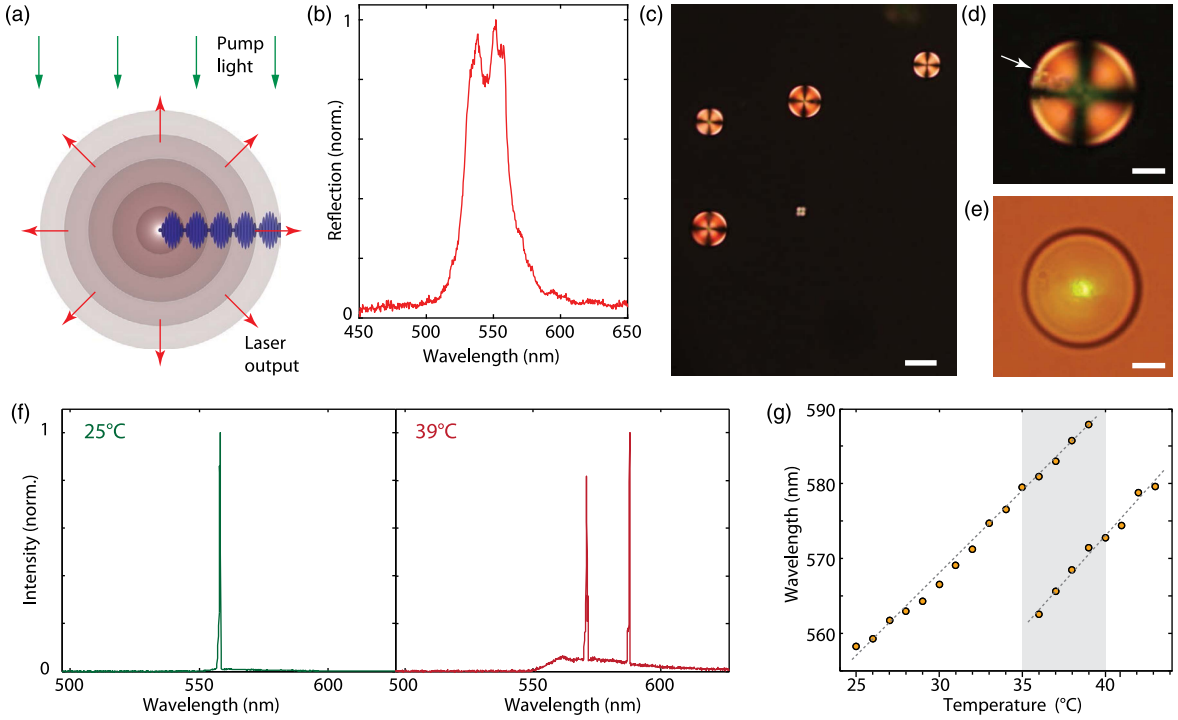

Fig. 4. Cholesterol lasers. (a) Schematic of a dye-doped cholesterol droplet. When optically pumped, the periodic liquid crystal helix supports optical resonance in the radial direction. (b) Reflection spectra from a 100 μm thick layer of cholesterol, which did not contain any dye. (c) Cholesterol droplets in glycerol between crossed polarizers. (d) A single droplet between crossed polarizers with the defect line visible. Arrow indicates the topological defect line. (e) Lasing from a single droplet is observed as a bright spot in the center of the droplet. Weak background light and pulsed laser were used to illuminate the droplet. (f) Lasing spectra at 25°C and 39°C. (g) Positions of the lasing peaks at the short and long bandedges as a function of temperature. The shaded area is the physiologically relevant temperature range. Scale bars are 50 μm in (b) and 20 μm in (c) and (d).

independent of the droplet size, but only on the periodicity. The standard deviation of the lasing wavelength across different droplets is only ~1 nm. This enables a more convenient platform for sensing than WGM, where a reference spectrum should be measured for each bead laser, due to unknown diameter, before the sensing is performed. The cholesteric pitch and, therefore, the periodicity of cholesteric liquid crystals is highly dependent on temperature. The lasing peaks increase almost linearly with the environmental temperature, with slopes of 2.2 and 2.4 nm/K for the long and short bandedge lines, respectively [Fig. 4(g)]. The lasers in water solution were stable on the shelf for a few days after preparation of the droplets, but completely dissolved in water within few weeks. Cholesterol droplets alone are not directly applicable to tissues because they coalescence with the surrounding tissue. If introduced into blood, the red blood cells aggregate to the droplet surface, changing their internal structure. For future use in biological environments, the cholesterol droplets will have to be coated with a shell or embedded in a solid matrix.

3. CONCLUSIONS

We have demonstrated biocompatible and biodegradable lasers in the forms of solid microbeads and liquid microdroplets. The implantable lasers have several advantages compared to just fluorescence. Narrow laser emission lines may enable more sensitive sensing, barcoding, and multiplexing. Even within tissues where there is strong scattering, the spectral lines' wavelength positions are insensitive to scattering and absorption. Therefore, even though we are unable to image the laser in the tissue, to determine its shape and exact position, the spectral lines still carry useful information. Solid-state microlasers were suitable for operation both in soft solid tissues and in blood. Liquid crystal Bragg onion lasers had a linear temperature dependence in the lasing wavelengths, offering the possibility of temperature sensing, but can be made also temperature insensitive by polymerizing into solid spheres [34,35]. The periodicity of polymerized cholesteric liquid crystals can be made sensitive to a variety of analytes, including metal ions [36,37], amino acids [38], and pH [39], for chemical and biomolecular sensing applications. In this work, synthetic dyes were employed as gain material, but other biocompatible materials could be used, for example, fluorescent proteins [40,41], vitamins [16], and medically approved dyes (Fluorescein and Indocyanine Green). Availability of biocompatible and biodegradable microlasers made from materials approved for medical use or substances already present in the human body may open new opportunities for light-based diagnostics and therapies [42], as well as basic research.

Funding. National Institutes of Health (NIH) (DP1-OD022296, P41-EB015903); National Science Foundation (NSF) (CMMI-1562863, ECCS-1505569); FP7 People: Marie-Curie Actions (PEOPLE) (627274); H2020 Marie Skłodowska-Curie Actions (MSCA) (702715).

REFERENCES

1. X. Fan and S.-H. Yun, "The potential of optofluidic biolasers," Nat. Methods **11**, 141–147 (2014).
2. M. Humar, S. J. J. Kwok, M. Choi, S. Cho, A. K. Yetisen, and S.-H. Yun, "Towards biomaterial-based implantable photonic devices," Nanophotonics **6**, 414–434 (2017).
3. Y. Sun and X. Fan, "Distinguishing DNA by analog-to-digital-like conversion by using optofluidic lasers," Angew. Chem. (Int. Ed.) **51**, 1236–1239 (2012).
4. M. Humar and S. H. Yun, "Intracellular microlasers," Nat. Photonics **9**, 572–576 (2015).
5. S. Cho, M. Humar, N. Martino, and S. H. Yun, "Laser particle stimulated emission microscopy," Phys. Rev. Lett. **117**, 193902 (2016).
6. M. C. Gather and S. H. Yun, "Single-cell biological lasers," Nat. Photonics **5**, 406–410 (2011).
7. M. Humar, M. C. Gather, and S.-H. Yun, "Cellular dye lasers: lasing thresholds and sensing in a planar resonator," Opt. Express **23**, 27865–27879 (2015).
8. Y.-C. Chen, Q. Chen, T. Zhang, W. Wang, and X. Fan, "Versatile tissue lasers based on high-Q Fabry-Pérot microcavities," Lab Chip **17**, 538–548 (2017).
9. M. Schubert, A. Steude, P. Liehm, N. M. Kronenberg, M. Karl, E. C. Campbell, S. J. Powis, and M. C. Gather, "Lasing within live cells containing intracellular optical micro-resonators for barcode-type cell tagging and tracking," Nano Lett. **15**, 5647–5652 (2015).
10. H. Cao, Y. Zhao, S. Ho, E. Seelig, Q. Wang, and R. Chang, "Random laser action in semiconductor powder," Phys. Rev. Lett. **82**, 2278–2281 (1999).
11. R. C. Polson and Z. V. Vardeny, "Random lasing in human tissues," Appl. Phys. Lett. **85**, 1289–1291 (2004).
12. E. I. Galanzha, R. Weingold, D. A. Nedosekin, M. Sarimollaoglu, J. Nolan, W. Harrington, A. S. Kuchyanov, R. G. Parkhomenko, F. Watanabe, Z. Nima, A. S. Biris, A. I. Plekhanov, M. I. Stockman, and V. P. Zharov, "Spaser as a biological probe," Nat. Commun. **8**, 15528 (2017).
13. C. Vannahme, F. Maier-Flaig, U. Lemmer, and A. Kristensen, "Single-mode biological distributed feedback laser," Lab Chip **13**, 2675–2678 (2013).
14. Y. Choi, H. Jeon, and S. Kim, "A fully biocompatible single-mode distributed feedback laser," Lab Chip **15**, 642–645 (2015).
15. A. Jonas and A. Kiraz, "In vitro and in vivo biolasing of fluorescent proteins suspended in liquid microdroplet cavities," Lab Chip **14**, 3093–3100 (2014).
16. S. Nizamoglu, M. C. Gather, and S. H. Yun, "All-biomaterial laser using vitamin and biopolymers," Adv. Mater. **25**, 5943–5947 (2013).
17. Y.-L. Sun, Z.-S. Hou, S.-M. Sun, B.-Y. Zheng, J.-F. Ku, W.-F. Dong, Q.-D. Chen, and H.-B. Sun, "Protein-based three-dimensional whispering-gallery-mode micro-lasers with stimulus-responsiveness," Sci. Rep. **5**, 12852 (2015).
18. M. Humar and S. H. Yun, "Whispering-gallery-mode emission from biological luminescent protein microcavity assemblies," Optica **4**, 222–228 (2017).
19. F. Vollmer and S. Arnold, "Whispering-gallery-mode biosensing: label-free detection down to single molecules," Nat. Methods **5**, 591–596 (2008).
20. M. Humar, A. Upadhya, and S. H. Yun, "Spectral reading of optical resonance-encoded cells in microfluidics," Lab Chip **17**, 2777–2784 (2017).
21. S.-K. Kang, R. K. J. Murphy, S.-W. Hwang, S. M. Lee, D. V. Harburg, N. A. Krueger, J. Shin, P. Gamble, H. Cheng, S. Yu, Z. Liu, J. G. McCall, M. Stephen, H. Ying, J. Kim, G. Park, R. C. Webb, C. H. Lee, S. Chung, D. S. Wie, A. D. Gujar, B. Vemulapalli, A. H. Kim, K.-M. Lee, J. Cheng, Y. Huang, S. H. Lee, P. V. Braun, W. Z. Ray, and J. A. Rogers, "Bioresorbable silicon electronic sensors for the brain," Nature **530**, 71–76 (2016).
22. V. D. Ta, S. Caixeiro, F. M. Fernandes, and R. Sapienza, "Microsphere solid-state biolasers," Adv. Opt. Mater. **5**, 1601022 (2017).
23. S. Nizamoglu, M. C. Gather, M. Humar, M. Choi, S. Kim, K. S. Kim, S. K. Hahn, G. Scarcelli, M. Randolph, R. W. Redmond, and S. H. Yun, "Bioabsorbable polymer optical waveguides for deep-tissue photomedicine," Nat. Commun. **7**, 10374 (2016).
24. S. Freiberg and X. X. Zhu, "Polymer microspheres for controlled drug release," Int. J. Pharm. **282**, 1–18 (2004).
25. H. K. Makadia and S. J. Siegel, "Poly lactic-co-glycolic acid (PLGA) as biodegradable controlled drug delivery carrier," Polymers **3**, 1377–1397 (2011).
26. H. Coles and S. Morris, "Liquid-crystal lasers," Nat. Photonics **4**, 676–685 (2010).

27. M. Humar and I. Muševič, "3D microlasers from self-assembled cholesteric liquid-crystal microdroplets," Opt. Express **18**, 26995–27003 (2010).
28. S. Furumi, S. Yokoyama, A. Otomo, and S. Mashiko, "Control of photonic bandgaps in chiral liquid crystals for distributed feedback effect," Thin Solid Films **499**, 322–328 (2006).
29. C. F. Soon, M. Youseffi, N. Blagden, R. Berends, S. B. Lobo, F. A. Javid, and M. Denyer, "Characterization and biocompatibility study of nematic and cholesteryl liquid crystals," in *Proceedings of the World Congress on Engineering* (2009), Vol. **2**, pp. 1872–1875.
30. C. F. Soon, W. I. W. Omar, R. F. Berends, N. Nayan, H. Basri, K. S. Tee, M. Youseffi, N. Blagden, and M. C. T. Denyer, "Biophysical characteristics of cells cultured on cholesteryl ester liquid crystals," Micron **56**, 73–79 (2014).
31. Y.-C. Chen, Q. Chen, and X. Fan, "Lasing in blood," Optica **3**, 809–815 (2016).
32. D. Seč, T. Porenta, M. Ravnik, and S. Žumer, "Geometrical frustration of chiral ordering in cholesteric droplets," Soft Matter **8**, 11982–11988 (2012).
33. G. Posnjak, S. Čopar, and I. Muševič, "Points, skyrmions and torons in chiral nematic droplets," Sci. Rep. **6**, 26361 (2016).
34. G. Cipparrone, A. Mazzulla, A. Pane, R. J. Hernandez, and R. Bartolino, "Chiral self-assembled solid microspheres: a novel multifunctional microphotonic device," Adv. Mater. **23**, 5773–5778 (2011).
35. M. Humar, F. Araoka, H. Takezoe, and I. Muševič, "Lasing properties of polymerized chiral nematic Bragg onion microlasers," Opt. Express **24**, 19237–19244 (2016).
36. M. Moirangthem, R. Arts, M. Merkx, and A. P. H. J. Schenning, "An optical sensor based on a photonic polymer film to detect calcium in serum," Adv. Funct. Mater. **26**, 1154–1160 (2016).
37. S. Kado, Y. Takeshima, Y. Nakahara, and K. Kimura, "Potassium-ion-selective sensing based on selective reflection of cholesteric liquid crystal membranes," J. Incl. Phenom. Macrocycl. Chem. **72**, 227–232 (2012).
38. P. V. Shibaev, D. Chiappetta, R. L. Sanford, P. Palffy-Muhoray, M. Moreira, W. Cao, and M. M. Green, "Color changing cholesteric polymer films sensitive to amino acids," Macromolecules **39**, 3986–3992 (2006).
39. P. V. Shibaev, R. L. Sanford, D. Chiappetta, and P. Rivera, "Novel color changing pH sensors based on cholesteric polymers," Mol. Cryst. Liq. Cryst. **479**, 161–167/1199–1205 (2007).
40. M. C. Gather and S. H. Yun, "Bio-optimized energy transfer in densely packed fluorescent protein enables near-maximal luminescence and solid-state lasers," Nat. Commun. **5**, 5722 (2014).
41. Q. Chen, M. Ritt, S. Sivaramakrishnan, Y. Sun, and X. Fan, "Optofluidic lasers with a single molecular layer of gain," Lab Chip **14**, 4590–4595 (2014).
42. S. H. Yun and S. J. J. Kwok, "Light in diagnosis, therapy and surgery," Nat. Biomed. Eng. **1**, 0008 (2017).